**NURETH14-169** 

## ANALYSIS ON THERMAL LOAD RESPONSE FOR THE IN-VESSEL RETENTION DURING A SEVERE ACCIDENT

**A. Jae Ryong Lee<sup>1</sup>, B. Rae Joon Park<sup>1</sup> and C. Seong Wan Hong<sup>1</sup>** Korea Atomic Energy Research Institute, Daejeon, South Korea

#### **Abstract**

A thermal load from the molten pool in the lower plenum to the reactor vessel during a severe accident has been analyzed. The configuration of the molten pool was considered as a two-layer. A heat flux distribution, crust thickness and vessel thickness were mainly investigated in this study. Non-linear Newton-Raphson iteration method was easily applied to solve a set of governing equations. Of many severe accident sequences, SBLOCA (Small Break Loss-Of-Coolant Accident) and LBLOCA (Large Break Loss-Of-Coolant Accident) without SI (Safety Injection) in the APR1400 were considered. From the results, the focusing effect in light metallic layer could be seen and other important parameter was also explained.

#### 1. Introduction

A thermal load response from a molten pool to the outer RPV (Reactor Pressure Vessel) in the lower plenum during a severe accident is very important to evaluate reactor vessel failure mechanism and to determine the safety margin for an IVR-ERVC (In-Vessel corium Retention through External Reactor Vessel Cooling) success. The Thermal load analysis is concentrated on a heat flux distribution in consideration of a thermal barrier effect in the thin metallic layer. A focusing effect of the metallic layer is mainly determined by the molten pool configuration in the lower head of the RPV. The melt pool configuration inside the lower plenum of the RPV affects an initial thermal load to the outer RPV and plays a key role to determine the integrity of the reactor vessel.

Of the previous researches to evaulate the robustness of the RPV, INEEL [1] developed the VESTA model for the thermal response of the lower head. In the ref [1], they examined the vessel integrity by using UCSB-assumed FIBS. Esmaili et al [2] derived a simple mechanistic model based on the existing constitutive relations and investigated the vessel failure for AP1000. Kim et al. [3] developed FVM-based module, named LILAC-meltpool, to simulate thermohydraulic behaviour of core melt relocated in the lower vessel during severe accident. LILAC-meltpool is based on an unstructured mesh technology to discretize solution domain of the vessel and molten pool. Kim et al. [4] derived LILAC-LP (lumped-parameter) that is simple approach for an analysis of the molten pool and investigated various accident scenarios in the APR1400 (Advanced Power Reactor 1400MWe).

In this study, a numerical model for thermal load response to the outer RPV during a severe accident has been adopted as a similar procedure of ref [2]. The governing equations were solved

using a non-linear Newton-Raphson method. The numerical scheme and heat transfer correlation used in this study was benchmarked against the results of other studies [1, 2] for AP600. The present results were good agreement with other results in the benchmark analysis. Finally, a thermal load response in the lower plenum of the APR1400 reactor vessel was analysed. Initial conditions such as corium mass and composition, volumetric heat source of the decay heat were achieved from the SCDAP/RELAP5 and GEMINI calculation. [5] A configuration of the molten pool in the lower plenum of the APR1400 RPV was assumed as a two-layer melt pool with a light metallic layer of Fe-Zr on top of a ceramic pool of UO2-ZrO2. The heat flux distribution from the molten pool to the outer RPV was determined from the thermal load analysis of the APR1400.

#### 2. Mathematical Model

Figure 1 shows a conceptual schematic of the two-layered melt pool configuration. The upper layer is assumed to be a light metallic layer of Fe-Zr and the lower to be an oxidic layer of UO2-ZrO2. Since the metallic layer is assumed to contain no uranium, the heat generation is totally provided by lower oxidic layer. In this study, other configuration such as three layer system is not considered.

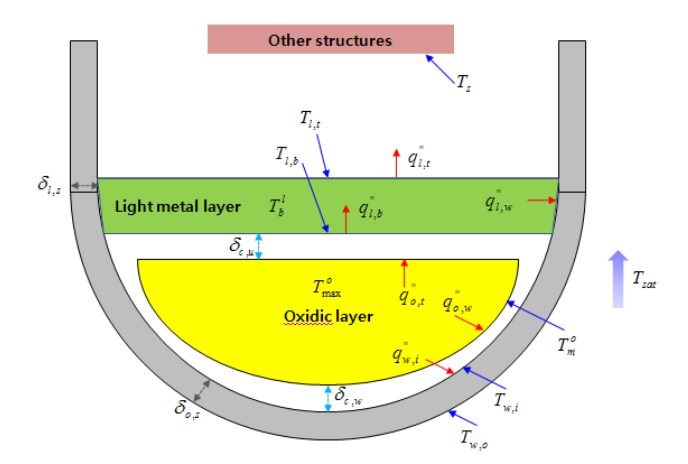


Figure 1 Schematic of the melt pool configuration in the lower head (two layers)

The governing equations for a given configuration as shown in Figure 1 are categorized into the conservation of energy equation in each layer and the heat flux equation between each layer with various heat transfer correlations.

## 2.1 Conservation of Energy

The conservation of energy equation in the lower oxidic layer and upper light metallic layer are as (1) and (2). In this study, the light metallic layer is considered to have no heat generation  $(Q_l^m = 0)$ . Equation (3) and (4) is energy balance in the upper and downward crust region, respectively. The heat generation of the crust is assumed to be same as one of the oxidic layer.

$$Q_{l}^{"}V_{l} + q_{l,b}^{"}A_{l,b} = q_{l,t}^{"}A_{l,t} + q_{l,w}^{"}A_{l,w}$$

$$(1)$$

$$Q_o^{"}V_o = q_{o,t}^{"}A_{o,t} + q_{o,w}^{"}A_{o,w}$$
 (2)

$$q_{l,b}^{"}A_{l,b} = Q_c^{"}V_{c,u} + q_{o,t}^{"}A_{o,t}$$
(3)

$$q_{w,i}^{"}A_{w,i} = q_{o,w}^{"}A_{o,w} + Q_{c}^{"}V_{c,w}$$
(4)

## 2.2 Heat Transfer in Oxidic Layer

In the two-layer configuration shown in Figure 1, the heat flux from the oxidic layer is distributed into upper light metal layer and the lower hemispheric vessel. First of all, the heat flux into the lower vessel wall is defined as (3).

$$q_{o,w}^{"} = h_{o,w}(T_{\text{max}}^{o} - T_{m}^{o})$$
 (5)

where  $T_{\text{max}}^o$  and  $T_{\text{m}}^o$  is the maximum temperature and the melting temperature of the oxidic layer, respectively. Since the crust is treated to have same amount of heat generation, the heat flux at the inner and outer boundary of the sideward crust can be expressed as follows;

$$q_{w,i}^{"} = \frac{k_c}{\delta_{c,w}} \left( T_m^o - T_{w,i} \right) - \frac{Q_c^{"} \delta_{c,w}}{2}$$
 (6)

$$q_{w,o}^{"} = \frac{k_c}{\delta_{cw}} \left( T_m^o - T_{w,i} \right) + \frac{Q_c^{"} \delta_{c,w}}{2}$$
 (7)

where  $q_{w,i}^*$  and  $q_{w,o}^*$  are the heat flux into the inner and outer vessel wall, respectively, and  $\delta_{c,w}$  is sideward crust thickness.

The heat flux through the vessel wall is simply expressed as the temperature difference between the inner and outer wall.

$$q_{w,i}^{"} = \frac{k_s}{\delta_{o,s}} \left( T_{w,i} - T_{w,o} \right) \tag{8}$$

where  $k_s$  and  $\delta_{o,s}$  are the thermal conductivity and the thickness of the vessel wall.

The heat flux from the vessel wall into the reactor cavity water,  $q_{w,o}^*$ , can be expressed by the following nucleate boiling relations;

$$q_{wi}^{"} = q_{wa}^{"} = C_{hoil} (T_{wa} - T_{sat})^3$$
 (9)

Where  $C_{boil}$  is the nucleate boiling coefficient and obtained from properties of saturated cavity water;

$$C_{boil} = \left(\frac{g[\rho_l - \rho_v]}{\sigma_l}\right)^{\frac{1}{2}} \left(\frac{c_{p,l}}{h_{fg}C_{sf} \operatorname{Pr}_l}\right)^3 (\mu_l h_{fg})$$
(10)

The other heat flux from the heat generation of the oxidic layer is transferred onto the upper light metallic layer;

$$q_{o,t}^{"} = h_{o,t}(T_{\text{max}}^{o} - T_{m}^{o}) \tag{11}$$

And the heat flux through the upper crust region is defined as the following form which is similar with (6) and (7).

$$q_{o,t}^{"} = \frac{k_c}{\delta_{c,u}} \left( T_m^o - T_b^l \right) - \frac{Q_c^{"} \delta_{c,u}}{2} \tag{12}$$

$$q_{l,b}^{"} = \frac{k_c}{\delta_{c,u}} \left( T_m^o - T_b^l \right) + \frac{Q_c^{"} \delta_{c,u}}{2}$$
(13)

#### 2.3 Heat Transfer in Light Metallic Layer

A thermal load from the light metallic layer is originally from the upward heat flux of the oxidic layer since the light metallic layer does not have any heat generation. That is why the heat flux from the light metallic layer is dependent on the upward heat transfer coefficient,  $h_{o,t}$ . The heat flux from the light metallic layer spreads two ways: upper structure, sideward vessel. At first, the upper surface heat flux can be obtained as;

$$q_{lt}^{"} = h_{lt}(T_h^l - T_{lt}) \tag{14}$$

where  $T_b^l$  is the bulk temperature of the metal pool, and  $T_{l,t}$  is the temperature of the upper surface of the light metallic layer. The heat transfer from the top surface of the light metallic layer to other structure in the RPV is assumed to be accomplished by radiation. Hence, the heat flux in (14) is also expressed as follows;

$$q_{l,t}'' = \frac{\sigma \left[ T_{l,t}^4 - T_s^4 \right]}{\left[ \frac{1}{\varepsilon_t} + \frac{1 - \varepsilon_s}{\varepsilon_s} \frac{A_{l,t}}{A_s} \right]}$$
(15)

Since the light metallic layer does not form the crust region at the contact area with sideward vessel wall, The heat flux from the light metallic layer to the sideward vessel wall can be simply obtained as;

$$q_{l,w}^{"} = h_{l,w}(T_b^l - T_m^{v}) \tag{16}$$

And also, the heat flux can be transferred through the vessel wall without any thermal loss since the vessel wall is considered to have no heat generation. Therefore, the heat flux through the vessel wall is provided as;

$$q_{l,w}^{"} = \frac{k_{w}}{\delta_{l,s}} (T_{m}^{v} - T_{w,o})$$
(17)

Where  $\delta_{l,s}$  is vessel thickness in the top metallic layer and considered to be same as  $\delta_{o,s}$  in this study. The heat flux to the outer water through the vessel wall is the same as  $q_{l,w}$ ;

$$q_{l,w}^{"} = h_{boil}(T_{w,o} - T_{sat}) = C_{boil}(T_{w,o} - T_{sat})^{3}$$
 (18)

The heat flux from the top oxidic crust to the light metallic layer,  $q_{l,b}^{"}$ , can be obtained as follows;

$$q_{lh}^{"} = h_{lh}(T_{lh} - T_{h}^{l}) \tag{19}$$

## 2.4 Solution methodology

At first, the heat partitioning from the heat generation of the oxidic layer into the lower hemispheric vessel wall and upper light metallic layer should be defined. By substituting (5) and (11) into (2), the maximum temperature,  $T_{\rm max}^o$ , becomes the only unknown variable by using the heat transfer coefficients from Table 1 so that it can be easily obtained. By inserting  $T_{\rm max}^o$  in (5) and (11) again, the heat flux onto both upper light metallic layer and the lower vessel wall can be calculated. It is important that since the heat partitioning into the upper side and the lower side is mathematically decoupled, the following procedure to obtain physical variables for the upward and downward is conducted separately.

For the heat partition to the lower hemispheric vessel wall, the main physical variables we are interested in are the heat flux to water, the inner/outer temperature and the crust thickness. Equations  $(6) \sim (9)$  are used to achieve these unknown variables. It should be noted that for this study, the angular variation of a heat transfer coefficient in the oxidic layer has been used. Therefore, since the heat flux and the crust thickness as well as the vessel wall thickness are a function of the heat transfer coefficient, they are also expressed as the angular variation form. Since the system of equations (6) through (9) is non-linear, it is solved by using a Newton-Raphson method as follows;

$$P^{(k)} = P^{(k-1)} - [J(P^{(k-1)})]^{-1} F(P^{(k-1)})$$
(20)

Where P, F(P) and J(P) are as follows;

$$P = \begin{bmatrix} T_{w,i} \\ \delta_{c,w} \\ T_{w,o} \\ q_{w,i} \end{bmatrix}, F(P) = \begin{bmatrix} 2\delta_{c,w}q_{o,w}^{"} - 2k_{c}(T_{m}^{o} - T_{w,i}) + Q_{c}^{"}\delta_{c,w}^{2} \\ 2\delta_{c,w}q_{w,i}^{"} - 2k_{c}(T_{m}^{o} - T_{w,i}) - Q_{c}^{"}\delta_{c,w}^{2} \\ \delta_{o,s}q_{w,i}^{"} - k_{s}(T_{w,i} - T_{w,o}) \\ q_{w,i}^{"} - C_{boil}(T_{w,o} - T_{sat})^{3} \end{bmatrix},$$

$$J(P) = \begin{bmatrix} 2k_{c} & 2Q_{o}^{m}\delta_{c,w} + 2q_{o,w}^{"} & 0 & 0 \\ 2k_{c} & -2Q_{o}^{m}\delta_{c,w} + 2q_{o,w}^{"} & 0 & 2\delta_{c,w} \\ -k_{c} & 0 & k_{c} & \delta_{o,s} \\ 0 & 0 & -3C_{boil}(T_{w,o} - T_{sat})^{2} & 1 \end{bmatrix},$$

$$(21)$$

The inner temperature of the vessel wall,  $T_{w,i}$ , should be less than a melting temperature of the vessel wall. If it exceeds the melting temperature of the vessel wall, then the inner wall is assumed to be ablating and the ablating thickness of the lower vessel wall should be calculated.

The procedure to obtain the physical variables involving the upper light metallic layer from the heat partition is same as those involving the lower vessel wall as explained above. Six unknown variables can be derived; heat fluxes, top/bottom surface temperate and bulk temperature, upper crust thickness, side vessel wall thickness and outer surface temperature of the vessel wall. Equations (11) through (19) are used to obtain the unknown variables.

## 3. RESULTS AND DISCUSSION

## 3.1 Results of Benchmarking Calculations

The present model described in above is compared with the results of the INEEL [1] and ERI [2] studies for AP600. The material properties and geometrical information are used in ref. [2]. Figure 2 shows the a few important physical variables from the benchmarking calculation. Figure 2(a)~(c) show the angular variation of the Heat flux to water, crust thickness and vessel wall thickness of the oxidic layer, whereas Figure 2(d)~(f) are informations for light metallic layer. All results are in good agreements with the previous references and even less than 5% error in the oxidic layer. In the Figure 2(a)~(c), both Park and Dhir [6] and mini-ACOPO correlations were considered as follows;

Park & Dhir : 
$$h_d(\theta) = \overline{h_d} \left( \frac{9.12(1 - \cos\theta_0)}{8 - 9\cos\theta_0 + \cos 3\theta_0} \sin^2 \theta + 0.24 \right)$$
 (22)

Mini-ACOPO : 
$$\frac{Nu_d}{\overline{Nu_d}} = \begin{bmatrix} 0.1 + 1.08 \left(\frac{\theta}{\theta_{tot}}\right) - 4.5 \left(\frac{\theta}{\theta_{tot}}\right)^2 + 8.6 \left(\frac{\theta}{\theta_{tot}}\right)^3 & for \ 0.1 \le \left(\frac{\theta}{\theta_{tot}}\right) \le 0.6 \\ 0.41 + 0.35 \left(\frac{\theta}{\theta_{tot}}\right) + \left(\frac{\theta}{\theta_{tot}}\right)^2 & for \ 0.6 \le \left(\frac{\theta}{\theta_{tot}}\right) \le 1.0 \end{bmatrix}$$

However, one could notice that the mini-ACOPO correlation was in good agreement with previous researches. The reason for differences in physical variables shown in Figure 2(d)~(f) is most likely due to the differences in the values for some of the parameter used in heat transfer coefficients.

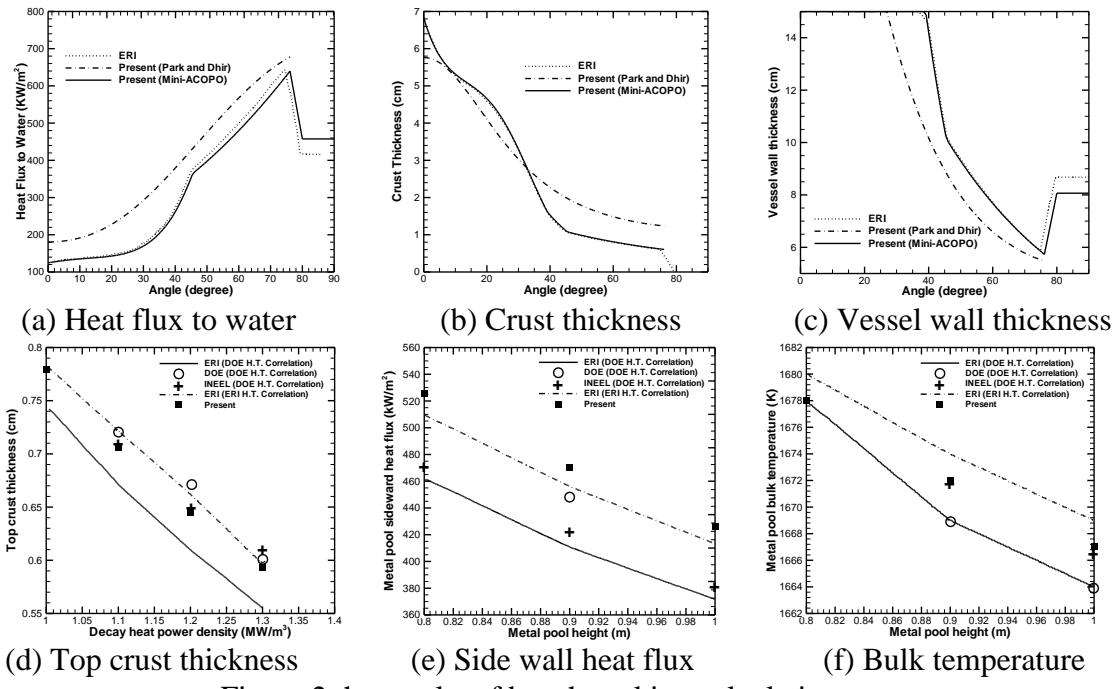


Figure 2 the results of benchmarking calculation

#### 3.2 Results of APR1400

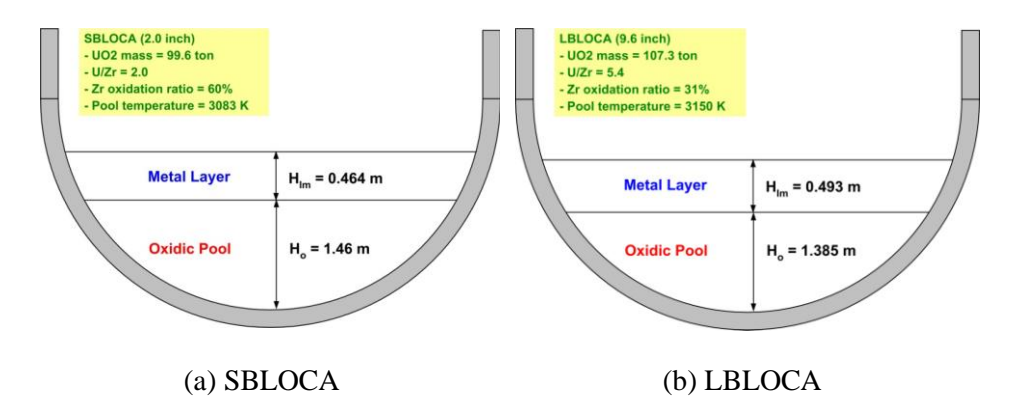


Figure 3 schematic for the relocation of melting pool of the APR1400

This study, of various severe accident scenarios, focused on the SBLOCA and LBLOCA without SI (Safety Injection) in the APR1400. The inner radius and thickness of the vessel are 2.37 m and 0.165 m, respectively. The thermal conductivity and melting temperature of the reactor vessel are 40.57 W/mK and 1760 K, respectively. The other geometrical configuration such as the height of each layer was obtained from the result of the GEMINI calculation which analyzes a thermodynamics phase diagram. [5] Figure 3 shows the schematics of two-layered configuration for both SBLOCA and LBLOCA of the APR1400. The heat generation from the oxidic layer was 2.2 MW/m³ for SBLOCA and 3.75 MW/m³ for LBLOCA which were achieved from the result of

SCDAP/REALP5. [5] The other data such as thermal properties of both layers were assumed to be same as given in benchmark calculation. [2] In this study, various combinations of the heat transfer correlations were estimated for the robustness of the reactor vessel. Table 1 is a set of heat transfer correlations used in this study. [2]

Table 1 Heat transfer correlation

Model		Top surface	Bottom surface	Side wall	
ERI Model	Metallic layer	Globe-Dropkin $Nu_l = 0.069 Ra_l^{0.333} Pr_l^{0.074}$	Globe-Dropkin $Nu_l = 0.069 Ra_l^{0.333} Pr_l^{0.074}$	Churchill-Chu $Nu_{I} = \left[0.825 + \left(\frac{0.387 Ra_{I}^{1/6}}{\left[1 + \left(0.492 / Pr_{I}\right)^{9/16}\right]^{9/27}}\right)\right]^{2}$	
ERI ]	Ceramic pool	Kulacki-Emara $Nu_d = 0.345 \left(Ra_{q,u}\right)^{0.226}$	Mayinger $Nu_d = 0.55 (Ra_{q,d})^{0.2}$		
DOE Model	Metallic layer	Globe-Dropkin "Specialized" $Nu = 0.15 Ra^{1/3}$	Globe-Dropkin "Specialized" $Nu = 0.15 Ra^{1/3}$	Churchill-Chu $Nu = 0.076 Ra^{1/3}$	
	Ceramic pool	$Nu_u = 0.345 Ra^{0.233}$	Mini-ACOPO $Nu_d = 0.0038Ra^{0.35} \left(\frac{H}{R}\right)^{0.25}$		
INEEL Model	Metallic layer	Globe-Dropkin $Nu_{l} = 0.069 Ra_{l}^{0.333} Pr_{l}^{0.074}$	Globe-Dropkin $Nu_{l} = 0.069 Ra_{l}^{0.333} Pr_{l}^{0.074}$	Churchill-Chu $Nu_{t} = \left[0.825 + \left(\frac{0.387 Ra_{t}^{1/6}}{\left[1 + \left(0.492 / Pr_{t}\right)^{9/16}\right]^{8/27}}\right)\right]^{2}$	
	Ceramic pool	ACOPO $Nu_u = 2.4415 Ra_p^{0.1772}$	ACOPO $Nu_d = 0.1857 Ra^{0.2304} \left(\frac{H}{R}\right)^{0.25}$		

First of all, the heat partitioning from the oxidic layer into the vessel wall and upper light metal layer is evaluated. Of various heat transfer correlations, three sets of correlations suggested by ERI, DOE and INEEL model are considered to evaluate the heat partitioning for the APR1400. Figure 4 shows the heat partitioning from the oxidic layer into the vessel wall and upper light metal layer. The ERI and DOE model show similar results and indicate that the heat flux into upper light metal layer is almost one and half times larger than that into lower vessel wall. Meanwhile, the INEEL model predicts the heat flux toward the metal layer about 15% larger than those of other two models. This is mainly because the heat transfer correlation toward the bottom vessel wall in INEEL predicts less than other two models.

Since the IVR phenomenon has been investigated in terms of focusing effect, it is far important to check the heat partitioning in the light metal layer. In this study, a few correlations are tested in order to evaluate the heat partitioning in the metal layer. For the given example such as 2-layer configuration, the heat partitioning from the decay heat of the ceramic pool is dependent on which heat transfer coefficient has been applied. And also, with considering focusing effect which may occur in the metal layer, it is desirable to expect less amount of heat flux toward metal layer. Among given models as shown in Figure 4, the INEEL model expects larger amount of heat flux toward metal layer than other two models.

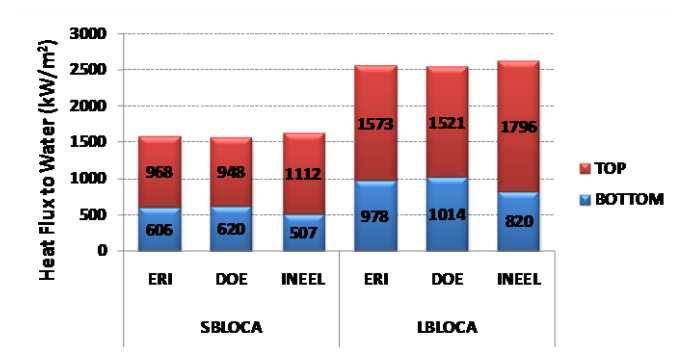
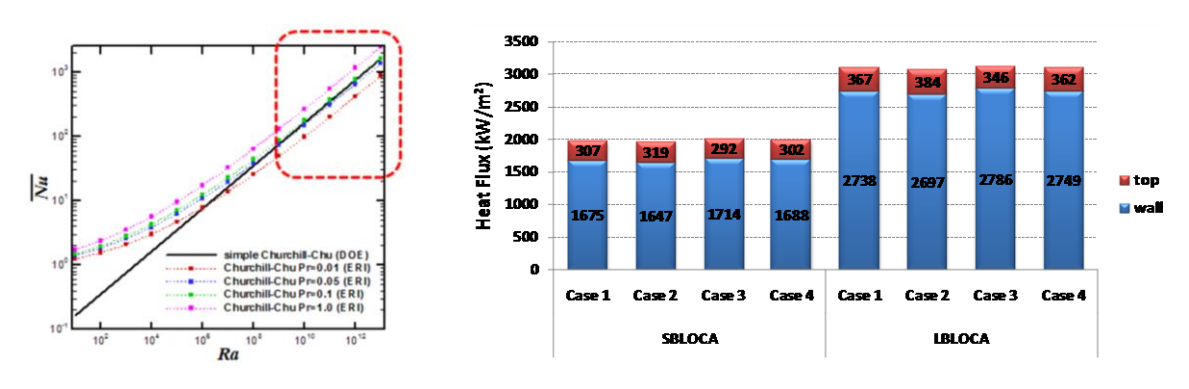


Figure 4 Heat partitioning in the ceramic layer

In the upper metal layer, the heat partitioning is more important than one in the oxidic layer. In this study, Globe-Dropkin for top/bottom surface and Churchill-Chu were only tested. The DOE model, however, had used far simplified correlation. Since the heat transfer correlation for side wall has been issued for the vessel failure mechanism, both Churchill-Chu correlation and simplified form was evaluated for a wide range of Pr and Ra. Figure 5(a) shows the profile of both correlations. One can notice that the simplified correlation is assumed to be agreement with Pr~0.1 for high Ra region. Since a Pr of a liquid metal is O(-2), the simplified correlation may expect less heat flux to the side wall than to the top.

Table 2 Combination of heat transfer coefficient for light metal layer

	Metal layer (T	op-Bottom)	Metal layer (Side)		
Case	Globe-Dropkin (ERI)	Globe-Dropkin "specialized" (DOE)	Churchill-Chu (ERI)	Simplified Churchill-Chu (DOE)	
1					
2					
3					
4					



(a) Profile for Churchill-Chu correlation

(b) Heat flux partitioning

Figure 5 Heat transfer partitioning for light metal layer

Before evaluating the heat partitioning in the light metal layer, a heat transfer correlation dependency was investigated. Table 2 is the combination of the heat transfer coefficient for both upper and side wall direction in the light metal layer and Figure 5(b) shows the result of heat flux partitioning. The energy transferred at upper surface is mainly by radiation heat transfer by eq. (15), whereas the sideward heat flux is caused by direct contact with the reactor vessel. Thus, the thermal energy is dominantly transferred into sideward vessel. And also, less sideward heat flux is observed in which simplified Churchill-Chu correlation is applied. (Case 2&4 in SBLOCA and LBLOCA, respectively)

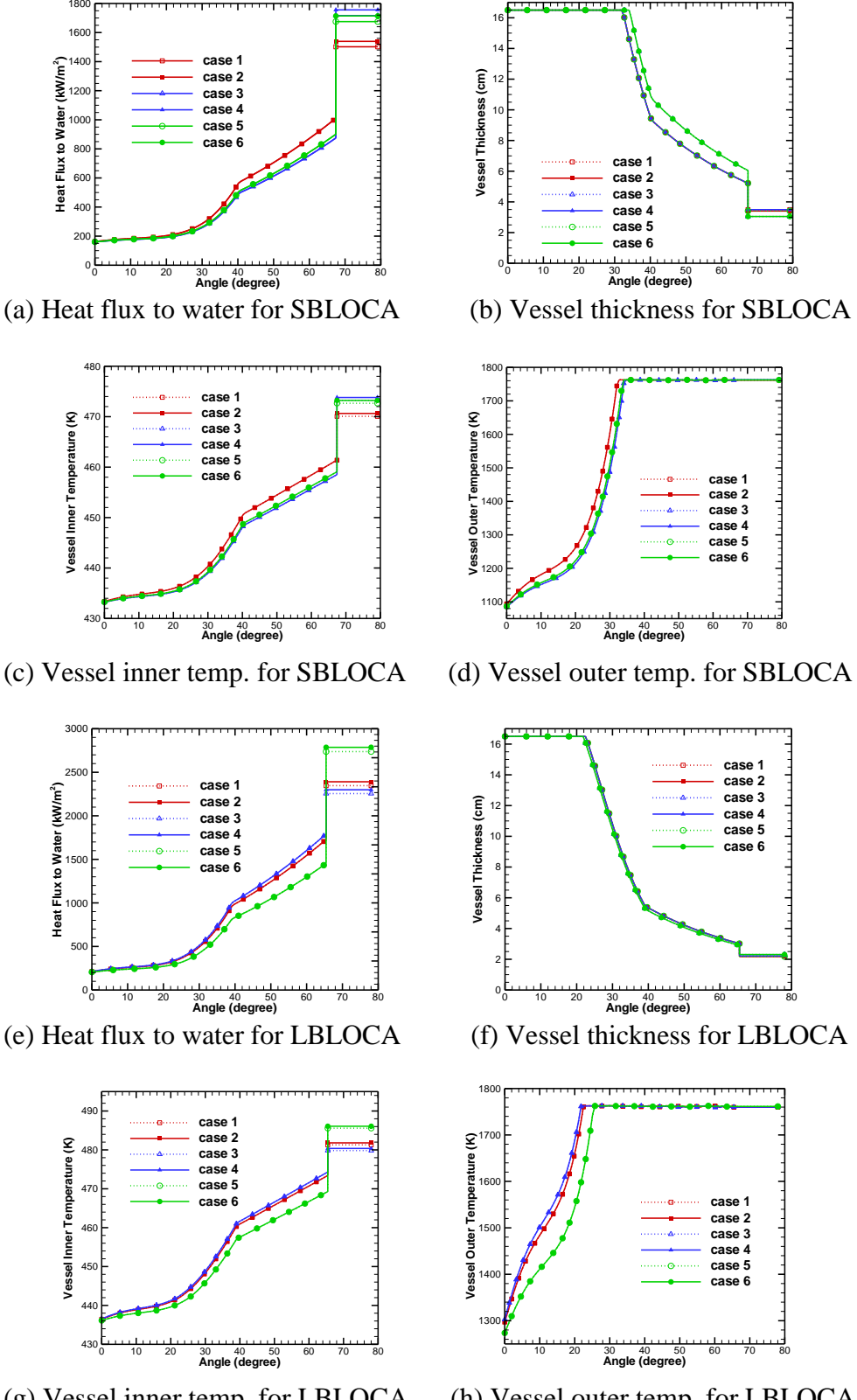
Finally, the dependency of the heat transfer correlations for whole layers was investigated. Table 3 shows the case option of which heat transfer coefficients are applied. In this calculation, Churchill-Chu was used for the sideward heat transfer coefficient for light metal layer for the conservative expectation of the heat flux to vessel wall. Figure 6 shows the heat flux to water and corresponding reactor vessel wall thickness as a function of the angle. The ERI model expected larger amount of the heat flux to water than those of other two in the oxidic layer region, whereas smallest amount in the metal layer regardless of which accident scenario it is. The DOE and INEEL model are observed to be almost same in the oxidic layer for heat flux to water as shown in the Figure 6(a). However, from the Figure 6(b), the vessel thickness profile indicates that ERI model does not differ from INEEL model. For the SBLOCA, the remaining thickness of the reactor vessel is about 3 cm. On the other hand, the scenario of the LBLOCA has the maximum heat flux to water at about 2700 kW/m² by using INEEL model in the ceramic layer and it has a possibility to be beyond the critical heat flux [2]. The reactor vessel, nevertheless, were still observed not to be failure. And also, the vessel thickness in the metal layer region for LBLOCA was not small compared with the result for SBLOCA.

Table 3 Combination of heat transfer coefficient for both layers

	C	eramic layer (Top)	Metal layer (Top-Bottom)		
Case	ERI model	DOE model	INEEL model	Globe-Dropkin	Globe-Dropkin "specialized"
1					
2					
3					
4					
5					
6					

#### 4. Conclusion

The thermal load response from the molten pool to the outer RPV (Reactor Pressure Vessel) in the lower plenum during a severe accident was analyzed with the conservation of energy equations. The heat partitioning from the oxidic layer, the crust formation and ablating of hemispheric vessel wall were physically defined. Non-linear Newton-Raphson iteration method was applied to solve the set of equations. In the lower oxidic pool region, the angular variation of heat transfer and crust thickness as well as vessel wall thickness was applied.



(g) Vessel inner temp. for LBLOCA (h) Vessel outer temp. for LBLOCA Figure 6 Physical variables for SBLOCA and LBLOCA

The scenario of SBLOCA and LBLOCA in the APR1400 were considered. Various sets of heat transfer correlations were applied to evaulate the vessel failure. Since the heat partition toward light metallic layer is larger than one to lower vessel, one can observed the heat flux to water has a quite large value. Thus, the focusing effect would be happed. Through both scenario, the reactor vessel was estimated and found that it did not happen to be failure.

Further physical models for other layer inversion such as upper oxidic layer on the heavy metallic layer or three-layered configuration should be investigated. And also, a variety of the heat transfer coefficients should be applied to make this simulation to be more realistic since the heat partitioning and corresponding heat fluxes are definitely dependent on the heat transfer coefficients. Since this study is just steady state analysis in terms of the comparison of various heat transfer correlations, a structural analysis such as a creep or thermal fatigue effect should be added for more realistic solution.

#### **Acknowledgments**

This work was supported by Nuclear Research & Development Program of the NRF (National Research Foundation of Korea) grant funded by the MEST (Ministry of Education, Science and Technology) of the Korean government (Grant code: M20702040004-08M0204-00410).

#### **Nomenclature**

A : Area

C : nucleate boiling coefficient

g : gravity acceleration

*h* : Heat transfer coefficient

*k* : thermal conductivity

Q : Heat generation

q: Heat flux

*T* : Temperature

V: Volume

## **Greek Symbols**

 $\alpha$ : Thermal diffusivity

 $\beta$ : Thermal expansion coefficient

 $\delta$  : thickness

 $\varepsilon$  : emmisivity

# The 14<sup>th</sup> International Topical Meeting on Nuclear Reactor Thermalhydraulics, NURETH-14 Toronto, Ontario, Canada, September 25-30, 2011

 $\rho$  : density

 $\sigma$  : Stefan-Boltzmann constant

v : kinematic viscosity

## Subscript

b : bulk

boil: boiling point

c : crust

l : light metal layer

*l,b* : bottom wall of light metal layer

*l,s* : vessel wall in the top metallic layer

*l,t* : top wall of light metal layer

*l,w* : side wall of light metal layer

m: melting

max : maximum

o : oxide pool

*o,s* : vessel wall in the oxide pool

*o,t* : top wall of oxide pool

s: internal structural area

sat : saturation

t: light metal layer – atmosphere

u : upper

w : vessel wall

w,i: inner wall of vessel

*w,o* : outer wall of vessel

## Superscript

" : per unit area

# The 14<sup>th</sup> International Topical Meeting on Nuclear Reactor Thermalhydraulics, NURETH-14 Toronto, Ontario, Canada, September 25-30, 2011

" : per unit volume

o : oxide pool

l : light metal layer

v : vessel

## References

- [1] Rempe, J. L. et al. (1997) "Potential for AP600 In-Vessel Retention through Ex-Vessel Flooding," INEEL.EXT-97-00779, Idaho falls, Idaho, USA
- [2] Esmaili, E. et al. (2004). "Analysis of In-Vessel Retension and Ex-Vessel Fuel Coolant Interaction for AP1000," NUREC/CR-6849, Rockvill, MD, USA
- [3] Kim, J.T. et al. (2002) "Development of LILAC-Meltpool for the thermo-hydraulic analysis of core melt relocated in a reactor vessel," KAERI/TR-2126/2002
- [4] S.B. Kim, et al., (2004) "Development of Optimal Severe Accident Management Strategy&Engineered Safety Features Development", KAERI/RR-2528/2004
- [5] R.J. Park, et al., "Analysis of severse accident progression for In-Vessel corium retention estimation in the APR1400", KAERI/TR-2664/2004
- [6] Park, H. and Dhir, V. K. (1992) "Effect of outside cooling on the thermal behavior of a pressurized water reactor vessel lower head," *Nuclear Technology*, **100**, pp.331